

Article

Numerical Simulating the Influences of Hydrate Decomposition on Wellhead Stability

Yuanfang Cheng¹, Mingyu Xue^{1,*} , Jihui Shi², Yang Li³, Chuanliang Yan¹, Zhongying Han¹ and Junchao Yang¹¹ School of Petroleum Engineering, China University of Petroleum (East China), Qingdao 266580, China² Sinopec Offshore Oil Engineering Co., Ltd., Shanghai 201206, China³ Sinopec Research Institute of Petroleum Engineering Co., Ltd., Beijing 102206, China

* Correspondence: myx875469168@163.com

Abstract: Natural gas hydrate reservoir has been identified as a new alternative energy resource which has characteristics of weak cementation, low reservoir strength and shallow overburden depth. Thus, the stability of subsea equipment and formation can be affected during the drilling process. To quantitatively assess the vertical displacement of the formation induced by hydrate decomposition and clearly identify the influence laws of various factors on wellhead stability, this study established a fully coupled thermo-hydro-mechanical-chemical (THMC) model by using ABAQUS software. The important factor that affects the wellhead stability is the decomposition range of hydrates. Based on this, the orthogonal experimental design method was utilized to analyze the influence laws of some factors on wellhead stability, including the thickness of hydrate formation, initial hydrate saturation, overburden depth of hydrate sediment, and mudline temperature. The results revealed that the decomposition of hydrate weakens the mechanical properties of the hydrate formation, thus leading to the compression of the hydrate formation, further causing the wellhead subsidence. When the duration of drilling operations was 24 h and no decomposition of natural gas hydrate occurs, the wellhead subsidence is recorded at 0.053 m, this value increases with an increase in drilling fluid temperature. The factors were listed in descending order as following, according to their significance of influences on wellhead stability: the thickness of hydrate formation, initial hydrate saturation, overburden depth of hydrate sediment, and mudline temperature. Among the above factors, statistical significance of the mudline temperature was less than 15% confidence level, suggesting that the effect of mudline temperature on wellhead stability is negligible. These findings not only confirm the influence of hydrate decomposition on wellhead stability, but also suggest important implications for the drilling of hydrate-bearing formation.

Keywords: natural gas hydrate; wellhead stability; numerical simulation; orthogonal design

Citation: Cheng, Y.; Xue, M.; Shi, J.; Li, Y.; Yan, C.; Han, Z.; Yang, J. Numerical Simulating the Influences of Hydrate Decomposition on Wellhead Stability. *Processes* **2023**, *11*, 1586. <https://doi.org/10.3390/pr11061586>

Academic Editor: Qingbang Meng

Received: 17 April 2023

Revised: 18 May 2023

Accepted: 18 May 2023

Published: 23 May 2023



Copyright: © 2023 by the authors. Licensee MDPI, Basel, Switzerland. This article is an open access article distributed under the terms and conditions of the Creative Commons Attribution (CC BY) license (<https://creativecommons.org/licenses/by/4.0/>).

1. Introduction

Natural gas hydrate is a cage-shaped, solid crystallized compound composed of methane and water molecules [1–4]. It has been widely found in the permafrost and seafloor sediments with specific temperature and pressure conditions [5–7]. During the complete decomposition of each volume of methane hydrate, about 160–180 volumes of methane in standard conditions are released, which means that the natural gas hydrate reservoirs contain a large amount of methane gas [8–10]. Due to its high energy density, wide distribution and cleanliness, natural gas hydrate has been recognized as an alternative energy source with great potential for development.

Interactions between drilling fluid in the drilling annulus space and hydrate formation will cause the temperature and pressure conditions changed during drilling which may break the phase equilibrium condition of hydrate [11–13]. As a result, the decomposition of hydrate occurred, weakening the strength of the hydrate formation. This could lead to wellhead subsidence and potential damage to equipment on the seabed [14,15], although

the inhibitors or nanoparticles application can reduce the range of hydrate decomposition [16]. However, drilling of hydrate-bearing formation remains a great engineering challenge [17,18]. Focusing on this engineering challenge, a large number of studies have been carried out for maintaining the stability of both formation and subsea equipment.

Wan et al. [19] established a 3D geological model of natural gas hydrate production to analyze the subsidence and stability of the reservoirs by depressurization, and based on this model pointed out that the decomposition of hydrate is the main reason which affects the reservoir subsidence. Yan et al. [20] performed a series of triaxial compressive tests on natural gas hydrate samples with different hydrate saturation, proving that the mechanical properties of hydrate formation changed with the decomposition of hydrates. Not only that, they also modified the Duncan-Chang hyperbolic model and obtained the constitutive model according with the deformation characteristics of natural gas hydrate formation. Li et al. [21] developed a thermo-hydro-mechanical coupling numerical model to contrast the stress fields and plastic zones before and after hydrate decomposition. Additionally, this study discussed the impact of hydrate decomposition on the wellbore stability. Zhang et al. [22] carried out a study on the stability of seabed caused by natural gas hydrate decomposition, and pointed out that the factors affecting the seabed instability are divided into external and internal factors. Fereidounpour and Vatani [23] designed and manufactured an experimental setup to study the mechanism of thermal stimulation. They claimed that drilling through natural gas hydrate formations can cause casing subsidence, which may result in the instability of the ocean floor

However, few studies have addressed the issue of wellhead stability caused by hydrate decomposition during drilling, and it remains unclear which factors can affect wellhead stability and the degree of influence. In this study, the focus is the influence analysis of hydrate dissociation on the stability of the wellhead. A fully coupled THMC model was established. Based on this model, the hydrate formation vertical displacement behavior under different drilling times and different drilling fluid temperature was analyzed. In addition, factors such as the thickness of hydrate formation, initial hydrate saturation, overburden depth of hydrate sediment, and mudline temperature affecting the wellhead stability were compared by orthogonal study.

2. Mathematical Principles

2.1. Natural Gas Hydrate Reaction Kinetics Equation

The kinetics of the hydrate dissociation reaction adopts the Kim-Bishnoi models, could be described by the following equation [24–26]:

$$\dot{m}_g = K_{rd}M_gA_{dec}(f_e - f_g) \quad (1)$$

$$\dot{m}_h = \dot{m}_g \frac{nM_w + M_g}{M_g} \quad (2)$$

$$\dot{m}_w = \dot{m}_g \frac{nM_w}{M_g} \quad (3)$$

where K_{rd} is intrinsic dissociation rate constant, $\text{mol}\cdot\text{m}^{-2}\cdot\text{Pa}^{-1}\cdot\text{s}^{-1}$; A_{dec} denotes the total surface area of hydrate decomposition per unit volume, m^{-1} ; M_g , M_w , M_h are the relative molecular mass of gas, water, hydrate, respectively, $\text{kg}\cdot\text{mol}^{-1}$; \dot{m}_g , \dot{m}_w , \dot{m}_h are the generation rate of gas and water and the hydrate assumption rate, respectively, $\text{kg}\cdot\text{m}^{-3}\cdot\text{s}^{-1}$; f_e is the gas fugacity in equilibrium with water and hydrate, Pa, and f_g is the local gas fugacity, Pa. In this paper, we use the equilibrium pressure and local gas pressure to characterize these variables, respectively. n denotes the coefficients of the decomposition reaction, dimensionless.

2.2. Mass Conservation Equations

The mass conservation equation of each component considering the influence of temperature and rock deformation on gas and water flow in porous media can be written as follows [27,28]:

$$\frac{\partial(\phi\rho_i S_i)}{\partial t} = -\nabla \cdot (\phi\rho_i S_i v_i) + \dot{m}_i + q_i \quad (4)$$

Use this equation to model the transport of multiple phases through the natural gas hydrate sediment, where ρ_i is the density of component i ($i = h, g, w$; h, g, w denote the hydrate phase, gas component and water component, respectively), $\text{kg}\cdot\text{m}^{-3}$; S_i, q_i, v_i are the saturation, source-sink term and velocity of component i , dimensionless, $\text{kg}\cdot\text{m}^{-3}\cdot\text{s}^{-1}$, $\text{m}\cdot\text{s}^{-1}$; ϕ is the effective porosity of hydrate formation, dimensionless, and can be written as:

$$\phi = \frac{1}{1 + \varepsilon_v}(\phi_0 + \varepsilon_v)$$

where ε_v is the volume strain, dimensionless; ϕ_0 is the effective porosity of the formation.

In this paper, we assume gas and water flow in porous media obey Darcy's law, which can be calculated by [29–31]:

$$v_j = -\frac{Kk_{rj}}{\mu_j}(\nabla P_j + \rho_j g) \quad (5)$$

K is the absolute permeability of porous media, mD, can be written as [32,33]:

$$K = K_0(1 - S_h)^N \quad (6)$$

K_0 is the original permeability of porous media without hydrate, mD; N is the permeability reduction index, dimensionless; μ_j, P_j are the viscosity and the phase pressure in pores of component j ($j = g, w$), Pa·s, Pa; k_{rj} denotes the relative permeability of component j , dimensionless.

2.3. Solid Mechanics Equations

The dynamic change of mechanical parameters in the process of hydrate decomposition is important basic data for the numerical simulation analysis of hydrate formation. With the dissociation of hydrate, the formation loses the support and cementation effect, which results in the decrease of elastic modulus and cohesion. The linear relationship between elastic modulus and hydrate saturation is expressed as follows: [34]:

$$E_{S_h} = E_0 + a_1 \cdot S_h \quad (7)$$

where E_0 is the elastic modulus of the formation rock when the saturation of hydrate is zero, MPa. In this paper, the constitutive model based on an improved Mohr-Coulomb criterion was used to build the relationship between effective stress and strain of the solid skeleton [35,36].

$$\tau = c_{S_h} + \sigma \tan \varphi \quad (8)$$

$$c_{S_h} = c_0 + \frac{1 - \sin \varphi}{2 \cdot \cos \varphi} \alpha \cdot (100 \cdot S_h)^\beta \quad (9)$$

where τ, c_{S_h}, σ and φ are the shear stress, cohesion of hydrate formation, confining pressure and internal friction angle, respectively, MPa, MPa, MPa, where c_0 denotes the cohesion of formation when the hydrate saturation is zero, MPa; α and β are material parameters, dimensionless.

Therefore, the critical value of the maximum principal stress on formation under different stress states can be written as:

$$\sigma_{1f} = \sigma_3 \cdot \tan^2\left(45^\circ + \frac{\varphi}{2}\right) + 2c_{S_h} \cdot \tan\left(45^\circ + \frac{\varphi}{2}\right) \quad (10)$$

where σ_{1f} represents the critical maximum principal stress, Pa, σ_3 is the minimum principal stress, Pa.

2.4. Energy Conservation Equations

Considering the heat conduction, heat convection and latent heat of hydrate decomposition, the energy conservation equation is as follows [37,38]:

$$\frac{\partial}{\partial t} \rho' C' = \nabla \cdot (\lambda_{\text{eff}} \nabla T) - \nabla \cdot (\rho_j C_j f S_j v_j) + Q \quad (11)$$

$$Q = -\dot{m}_h \Delta H \quad (12)$$

$$\rho' C' = (1 - \phi) \rho_s C_s + \sum \phi S_i \rho_i C_i \quad (13)$$

$$\lambda_{\text{eff}} = (1 - \phi) \lambda_s + \sum \phi S_i \lambda_i \quad (14)$$

where C_s and C_i are the specific heat of reservoir rock and component i , $\text{kJ} \cdot \text{kg}^{-1} \cdot \text{K}^{-1}$; λ_s , λ_i are the thermal conductivity of reservoir rock, component i , respectively, $\text{W} \cdot \text{m}^{-1} \cdot \text{K}^{-1}$; Q means the heat absorbed due to hydrate dissociation, $\text{W} \cdot \text{m}^{-3}$, ΔH is the enthalpy change of hydrate, can be written as [39,40]:

$$\Delta H = 446.12 \times 10^3 - 132.638T \quad (15)$$

3. Simulation Model and Experimental Design

3.1. Model Description

For simplifying this sophisticated model that includes phase change, heat transfer, and fluid flow, several assumptions or simplifications are made for this specific problem: (1) The natural gas hydrate formations involved in this model are assumed to be isotropic and homogeneous; (2) natural gas is considered to be an ideal gas that doesn't dissolve in water; and (3) there is no relative slip between the well surface casing and the formation, and the underwater wellhead settlement is entirely due to hydrate decomposition.

Based on the above assumptions and simplifications, the geometry of the established 2D axisymmetric simulation model is shown in Figure 1. The size of the sediment is 200 m in the X direction and 415 m in the Y direction. In the vertical direction, the model consists of three parts: 25 m for the natural gas formation and 195 m for the overlying formation and underlying formation. In the radial direction, the diameter and thickness of the surface case are 0.762 m (30 in) and 0.0254 m (1 in), respectively, and is located only in the overlying formation, allowing for heat transfer but no fluid flow between the drilling fluid and overlying formation. The wellbore exhibited a diameter of 0.6604 m (26 in) which is located in the natural gas hydrate formation.

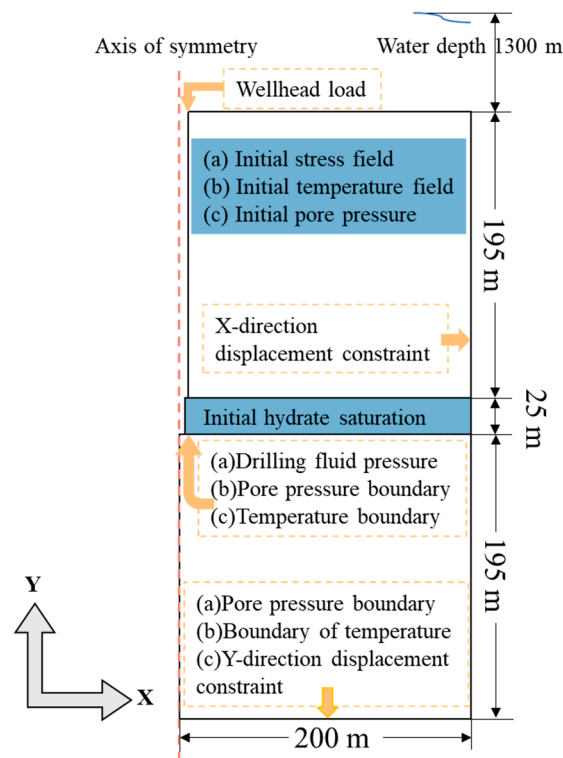


Figure 1. Schematic diagram of the geometric model and boundary/initial conditions.

The initial pore pressure state is assumed to be hydrostatic; the initial stress field is set as the lithostatic pressure at the corresponding depth, and the initial temperature field is estimated based on the geothermal gradient of the formation. These physical fields are all applied to the formation zones. Boundary conditions for the fluid column pressure and temperature of drilling fluids are established separately on the wellbore. Normal displacement of the right and bottom boundaries is constrained during the analysis.

The model calculation process consists of two steps. In the first step, the in-situ stress balance, which can obtain the equilibrium condition when the physic field is applied to the entire model. In the second step, the stability of the underwater wellhead can be analyzed by changing the boundary conditions. Moreover, the main parameters for the numerical modeling of our simulation are shown in Table 1 [41].

Table 1. Main parameters for numerical simulations.

Parameters	Value	Parameters	Value
Depth of water	1300 m	Water density	1000 kg·m ⁻³
Hydrate density	910 kg·m ⁻³	Rock grain density	2200 kg·m ⁻³
Water thermal conductivity	0.6 W·m ⁻¹ ·K ⁻¹	Water specific heat	4.2 kJ·kg ⁻¹ ·K ⁻¹
Rock grain thermal conductivity	1.5 W·m ⁻¹ ·K ⁻¹	Rock grain specific heat	1.6 kJ·kg ⁻¹ ·K ⁻¹
Hydrate thermal conductivity	0.4 W·m ⁻¹ ·K ⁻¹	Hydrate specific heat	2.1 kJ·kg ⁻¹ ·K ⁻¹
Methane gas thermal conductivity	0.00335 W·m ⁻¹ ·K ⁻¹	Methane gas specific heat	2.093 kJ·kg ⁻¹ ·K ⁻¹
Elastic modulus of sediment	35.414 MPa	Cohesion of sediment	0.1 MPa
Initial formation permeability	1 mD	Initial porosity	0.4246
Geothermal gradient	0.0456 K·m ⁻¹	Submarine water temperature (Mudline)	5.67 °C
Drilling fluid density	1000 kg·m ⁻³	Drilling fluid temperature	21.253 °C
Elastic modulus of casing	206.8 GPa	Poisson's ratio of casing	0.25
α	0.0011	β	1.91

3.2. Orthogonal Experimental Design

The orthogonal study is a scientific method that utilizes an orthogonal table to design the test scheme and analyze the test results. In this paper, the objective is to analyze the influence degree of each factor on subsea wellbore stability, and the index is the vertical displacement of the subsea wellbore. Four influencing factors include the initial hydrate saturation, thickness of hydrate formation, overburden depth of hydrate sediment, and mudline temperature, with four parameter levels determined for each factor, as shown in Table 2. The orthogonal study can reduce the total number of studies. Due to this advantage, a designed orthogonal study consisting of 16 representative dependent studies was therefore implemented to reduce the investigation number, as shown in Table 3.

Table 2. Factors and corresponding levels.

Factors	Value			
Initial hydrate saturation	0.15	0.3	0.45	0.6
The thickness of hydrate formation	10 m	20 m	30 m	40 m
Overburden depth of hydrate sediment	170 m	180 m	190 m	200 m
Mudline temperature	3 °C	4 °C	5 °C	6 °C

Table 3. Orthogonal experiment design.

	Initial Hydrate Saturation	Thickness of Hydrate Layer	Overburden Depth of Hydrates	Mudline Temperature
Case-1	0.15	10 m	170 m	3 °C
Case-2	0.15	20 m	180 m	4 °C
Case-3	0.15	30 m	190 m	5 °C
Case-4	0.15	40 m	200 m	6 °C
Case-5	0.3	10 m	180 m	5 °C
Case-6	0.3	20 m	170 m	6 °C
Case-7	0.3	30 m	200 m	3 °C
Case-8	0.3	40 m	190 m	4 °C
Case-9	0.45	10 m	190 m	6 °C
Case-10	0.45	20 m	200 m	5 °C
Case-11	0.45	30 m	170 m	4 °C
Case-12	0.45	40 m	180 m	3 °C
Case-13	0.6	10 m	200 m	4 °C
Case-14	0.6	20 m	190 m	3 °C
Case-15	0.6	30 m	180 m	6 °C
Case-16	0.6	40 m	170 m	5 °C

4. Simulation Results and Analysis

4.1. Relationship between the Stabilities of Wellhead and Drilling Time

Figure 2 shows the temperature distribution of the formation after drilling time of 6 h, 12 h and 24 h. For the convenience of observing the trend of temperature change in different positions (the top and bottom of natural gas hydrate formation), the mudline and the bottom of the model were selected.

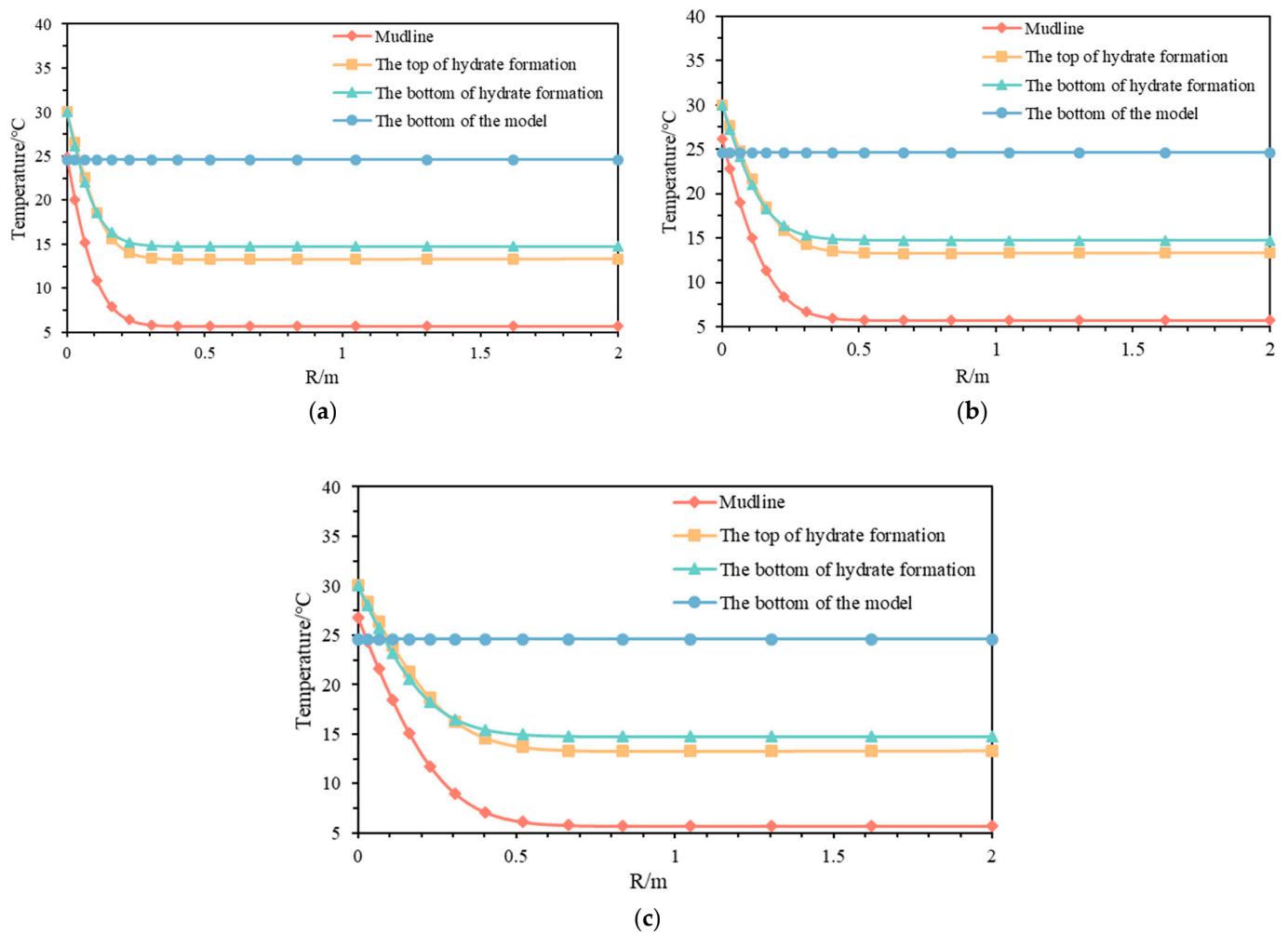


Figure 2. Relationship between formation temperature and distance to the borehole wall under different drilling fluid circulation time (a) 6 h (b) 12 h (c) 24 h.

The circulation of drilling fluid changes in the temperature distribution of the formation around the wellbore caused by heat transfer. It can be observed that the temperature rise rate at the mudline is lower compared to the natural gas hydrate formation, due to its lower initial temperature and heat transfer between formation and seawater. The temperature at the bottom of model remains constant because it has not been disturbed by engineering activities. It is worth noting that as time passed, the distance of the position where the formation was heated by drilling fluid from the borehole wall increased. The distance from the temperature change front to the wellbore at the bottom of the natural gas hydrate sediment was 0.52 m, 0.836 m and 1.048 m after drilling for 6, 12, 24 h, respectively.

The range of hydrate decomposition increases gradually as the influence range of drilling fluid temperature increases. Figure 3 shows that the distance between the hydrate decomposition front and wellbore at the middle of the hydrate formation was 0.2264 m, 0.3067 m and 0.367 m after drilling for 6, 12, 24 h, respectively.

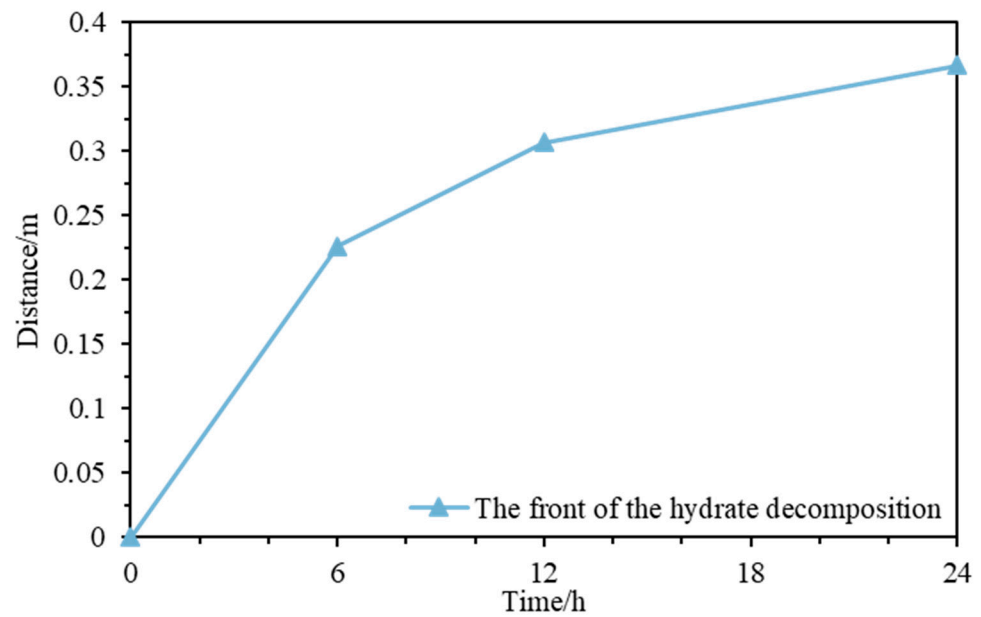


Figure 3. Relationship between the hydrate decomposition front and time.

The mechanical properties of the hydrate formation are positively correlated with the hydrate saturation. Based on this, under the same in-situ stress conditions, the formation will produce secondary compression consolidation with hydrate decomposition. The vertical displacement of the hydrate formation under different drilling fluid circulation times is shown in Figure 4. To better visualize the sediment geometry, the model deformation factor of 10 is used, and the near-wellbore areas at the top and bottom of the reservoir are selected ($6\text{ m} \times 4\text{ m}$). It can be observed that due to the decomposition of hydrate, the upper formation deforms downward and the lower formation deforms upward in the near-wellbore area. In addition, the uplift of the lower formation is greater than the subsidence of the upper formation. The reason for this phenomenon is that the upper formation bear more load caused by casing and underwear wellhead settlement in addition to the in-situ stress compared to the lower formation.

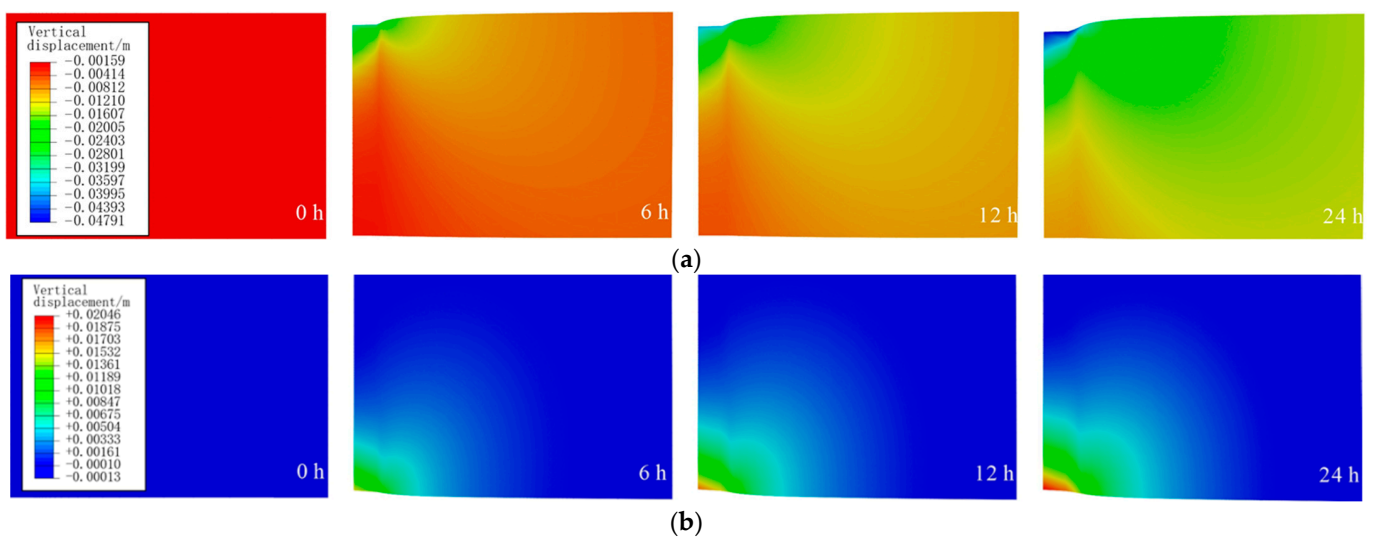


Figure 4. Vertical deformation of the natural gas hydrate formation for the different time (a) at the top of the formation and (b) at the bottom of the formation.

4.2. Relationship between the Stabilities of Wellhead and Drilling Fluid Temperature

Figure 5 shows the temperature distribution and hydrate saturation distribution in the middle of natural gas hydrate sediment after drilling for 24 h, when drilling fluid temperatures were 10 °C, 25 °C, 30 °C, 35 °C, and 40 °C. It can be observed that during the same time, with the increase of drilling fluid temperature, the range of formation temperature affected increased, resulting in a larger range of hydrate decomposition. Furthermore, due to the range of hydrate decomposition increased, the compression amplitude of natural gas hydrate sediment increased.

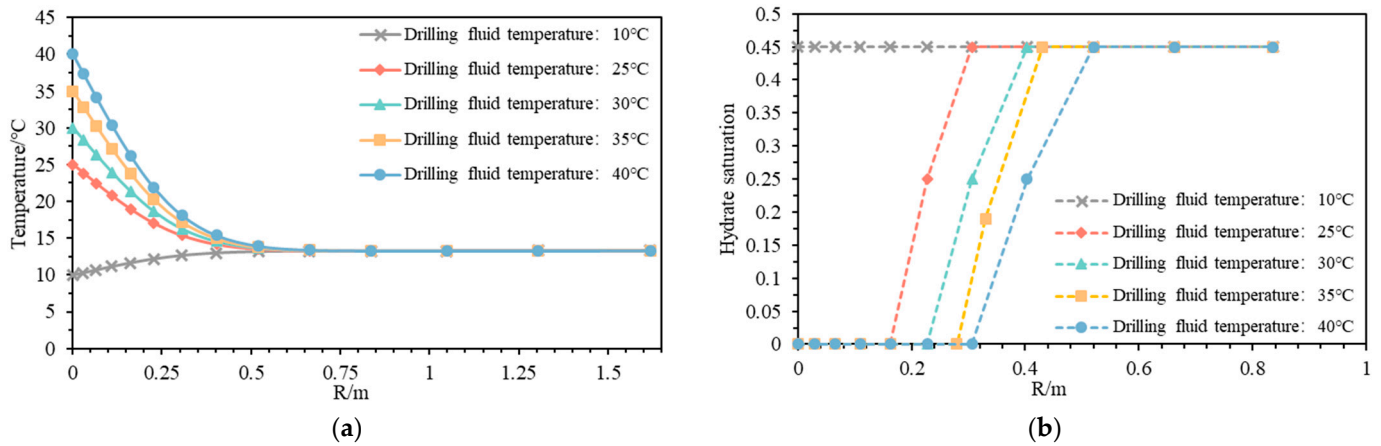


Figure 5. (a) Relationship between formation temperature and distance to the borehole wall at the middle of the hydrate formation and (b) relationship between hydrate saturation and distance to the borehole wall at the middle of the hydrate formation.

Figure 6 illustrates the vertical displacement of the top and bottom of the hydrate-bearing sediment. In the figures, it can be observed that when the drilling fluid temperature was 10 °C, the natural gas hydrate does not decompose under this state. This means that the accumulated compression (the sum of the vertical deformation at the top and bottom of the sediment) of the natural gas hydrate sediment was 0.006 m. When the drilling fluid temperature was 25 °C, the accumulated compression was 0.059 m, and when the drilling fluid temperature increased to 40 °C, this value reached 0.104 m. The increase of hydrate decomposition area will aggravate the subsea wellhead subsidence, as can be seen in Figure 7. It can be observed that the effect of the subsea wellhead load will lead to a small amount of consolidation and subsidence of the formation around the wellhead. As the time was 24 h, where no decomposition of natural gas hydrate occurs, the subsidence of the wellhead was 0.053 m. This value increases as the drilling fluid temperature increases.

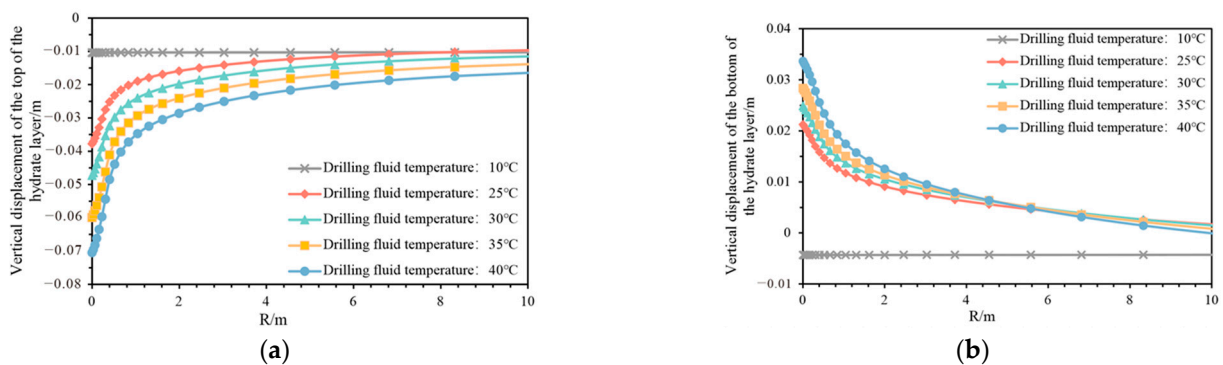


Figure 6. Relationship between vertical displacement and distance to the borehole wall (a) at the top of the hydrate formation and (b) at the bottom of the hydrate formation.

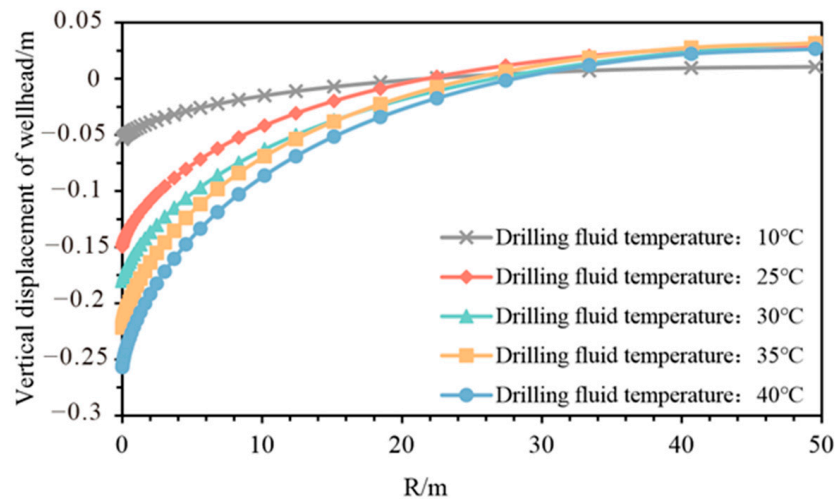


Figure 7. Relationship between subsea wellhead subsidence and distance to the borehole wall.

4.3. Range Analysis of Factors for Wellhead Stability

The range analysis of the influencing factors on the subsea wellbore stability is shown in Figure 8. Figure 8a shows the distribution of vertical displacement statistics under different experiment conditions. It can be observed that the influence trends and degrees of various factors on the subsea wellhead stability will be reflected under different influence conditions. For example, the increase in the thickness of the natural gas hydrate formation results in a large vertical displacement of the subsea wellhead. In contrast, the temperature of the mudline insignificantly impacts the stability of the subsea wellhead.

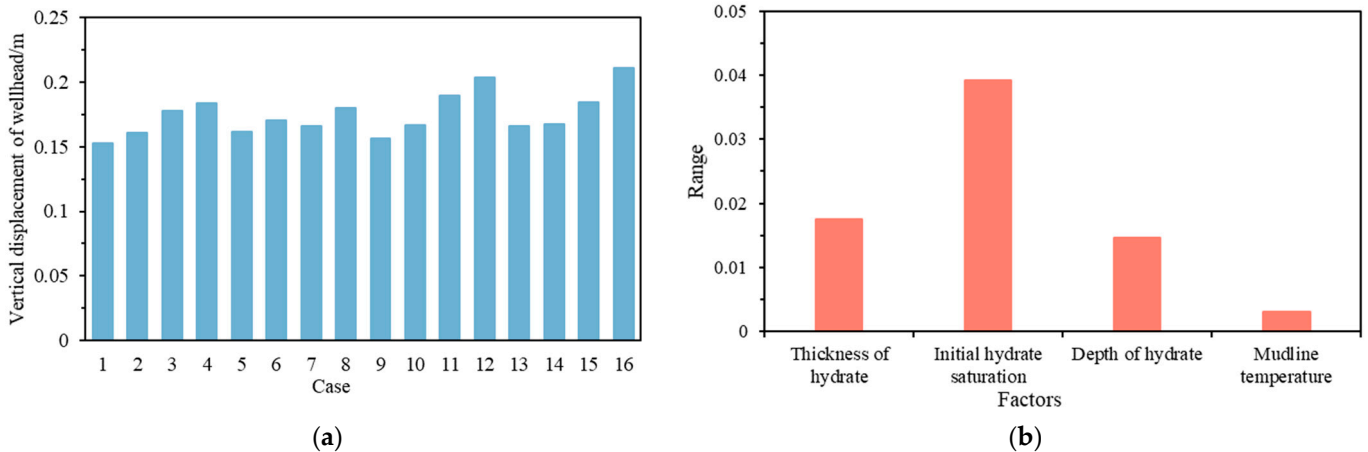


Figure 8. (a) Distribution of subsea wellhead subsidence under various factors and (b) range analysis on various factors.

Variance analysis was used to comprehensively evaluate the influence degree of the four factors on the subsea wellbore stability. Table 4 shows the test results of the inter-subject effect of the variance analysis of subsea wellhead subsidence, where the sum of squares and mean square reflect the effects of each factor on the index. The significance of the thickness of the hydrate layer is less than 0.01, indicating that the thickness of the hydrate layer has an extremely significant effect on the subsidence of the underwater wellhead. The significance of the hydrate saturation and the depth of the hydrate layer are 0.058 and 0.094, respectively, indicating that these two factors have a certain influence on underwater wellhead settlement. In contrast, the statistical significance of the mudline temperature was 0.854, which was less than a 15% confidence level, suggesting that the mudline temperature had no significant influence on the subsidence of the subsea wellhead. This is due to the fact that decomposition rate of hydrates is primarily influenced by the

heat transfer rate, which is mainly affected by the heat transfer between the drilling fluid and the formation. Although a small increase in the mudline temperature may cause a slight temperature rise in the reservoir, its impact on the heat transfer rate is relatively insignificant. Sensitivity evaluation of each factor was also performed, and Figure 8b shows that the influence order of these factors on the wellhead stability decreased in the following sequence: the thickness of the hydrate formation, the initial natural gas hydrate saturation, the depth of the hydrate formation and the temperature of the mudline.

Table 4. Analysis of variance.

Source	Type III SS	Freedom	Mean Square	F	Significance
Initial hydrate saturation	0.001	3	0	8.264	0.058
Thickness of hydrate formation	0.003	3	0.001	39.331	0.007
Depth of hydrate formation	0	3	0	5.689	0.094
Mudline temperature	2.09×10^{-5}	3	6.96×10^{-6}	0.255	0.854
Error	8.18×10^{-5}	3	2.73×10^{-5}		
Total	0.492	16			

4.4. Influence of Natural Gas Hydrate Sediment Thickness

Figure 9 shows the influence curves of the thickness of hydrate formation on the subsea wellhead subsidence. It can be seen from the figure that the subsidence of the subsea wellhead increased significantly with the growth of the thickness of natural gas hydrate formation. For example, when the thickness of the hydrate sediment was 10 m, the average value of subsea wellhead subsidence was 0.156 m, and when the thickness of the hydrate sediment was 40 m, this value increased to 0.1953 m.

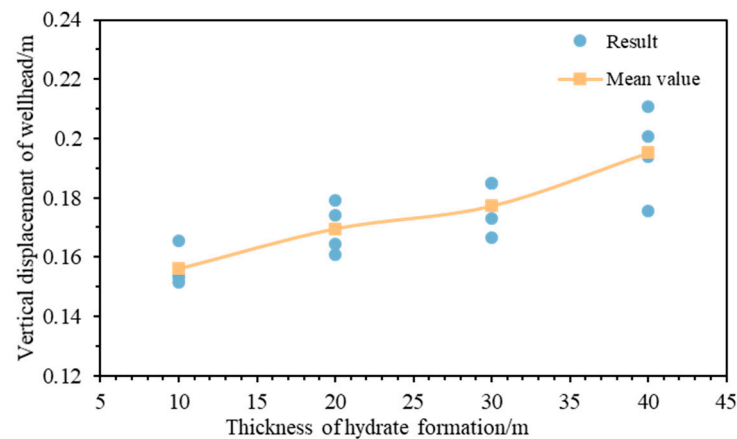


Figure 9. Relationship between subsea wellhead subsidence and hydrate formation thickness.

The reason for this result is that the heat transfer between the drilling fluid and hydrate sediment occurs during drilling, which leads to hydrate decomposition. The increase in hydrate formation thickness means that the volume of the contact zone between drilling fluid and hydrate formation increases during drilling, which causes growth of the volume of the zone where hydrates are decomposed. As a consequence, the effective pore volume caused by hydrate decomposition is increased, leading to the expansion of the low-strength zone. This, in turn, results in a greater compression deformation of the hydrate sediment. This observation is also supported by the vertical displacement at the top and bottom of the hydrate sediment in Case 5 and Case 8, as shown in Figure 10.

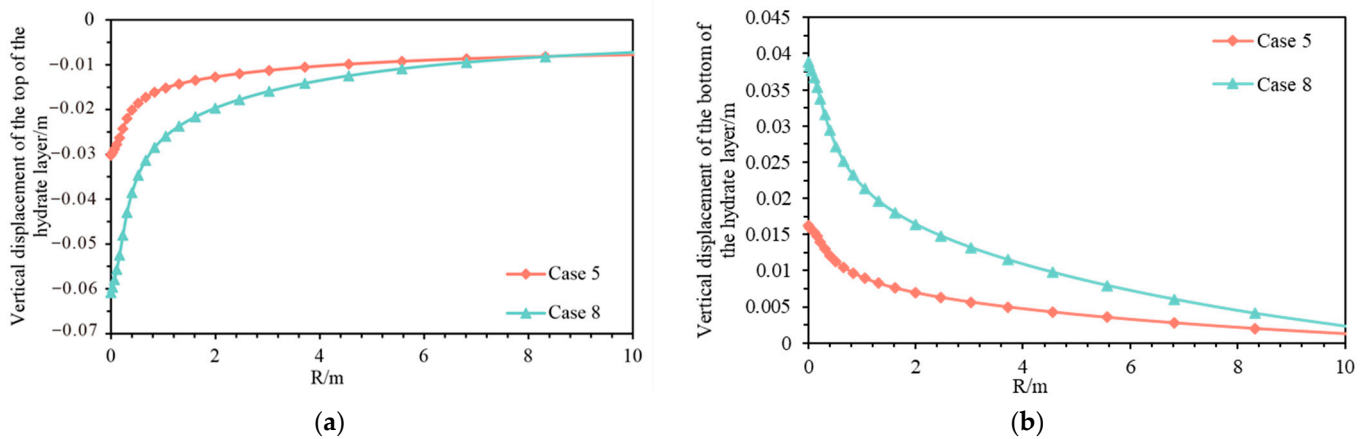


Figure 10. Relationship between vertical displacement and distance to the borehole wall under cases 5 and case 8: (a) at the top of the hydrate formation and (b) at the bottom of the hydrate formation.

4.5. Influence of Initial Hydrate Saturation

Figure 11 shows the influence curves between the initial saturation of the hydrate formation and the subsea wellhead subsidence. It can be seen from the figure that the subsidence of the subsea wellhead shows an approximately linear increase, with increasing initial hydrate saturation. For example, when the initial hydrate saturation was 0.15, the average value of subsea wellhead subsidence was 0.1646 m, and when the initial hydrate saturation was 0.6, this value increased to 0.1821 m.

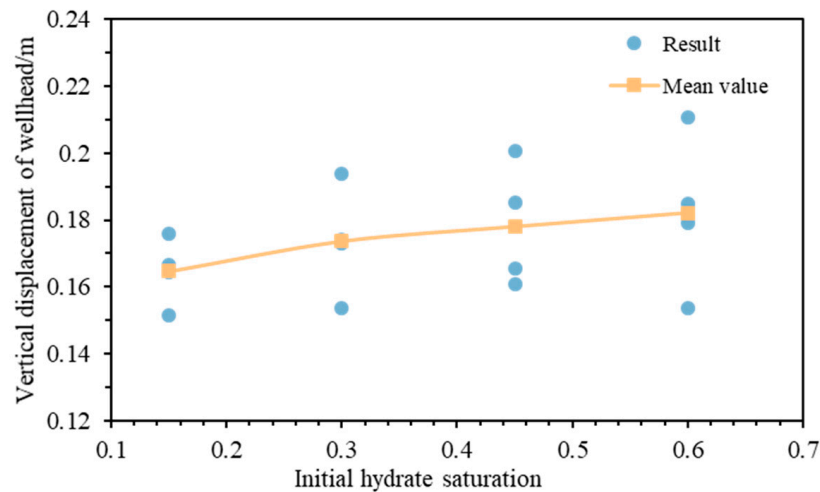


Figure 11. Relationship between subsea wellhead subsidence and initial hydrate saturation.

This result occurs mainly because of two aspects. On the one hand, this study assumes that the strength of the hydrate sediment is positively correlated with the saturation of the hydrate as shown in Equation (7). It is worth noting that the strengths of the hydrate sediment are identical when the hydrate saturation is zero. Therefore, the higher initial saturation of hydrate results, the larger the strength decrease of hydrate formation between before and after decomposition, which leads to greater deformation of the hydrate sediment to balance the in-situ stress between the overlying layer and the underlying layer. On the other hand, the higher the initial saturation of hydrate, the greater the pore volume change before and after the hydrate decomposition, leading to a larger void volume in the strata, resulting in larger subsea wellhead subsidence.

4.6. Influence of Hydrate Sediment Overburden Depth

Figure 12 shows the relationship between the overburden depth of hydrate formation and the subsea wellhead subsidence. It can be observed that the subsidence of the subsea

wellhead exhibits a negative correlation with the depth of hydrate sediment. For example, when the overburden depth of the hydrate sediment was 170 m, the average value of subsea wellhead subsidence was 0.1804 m, while this value decreased to 0.165 m when the depth reached 200 m.

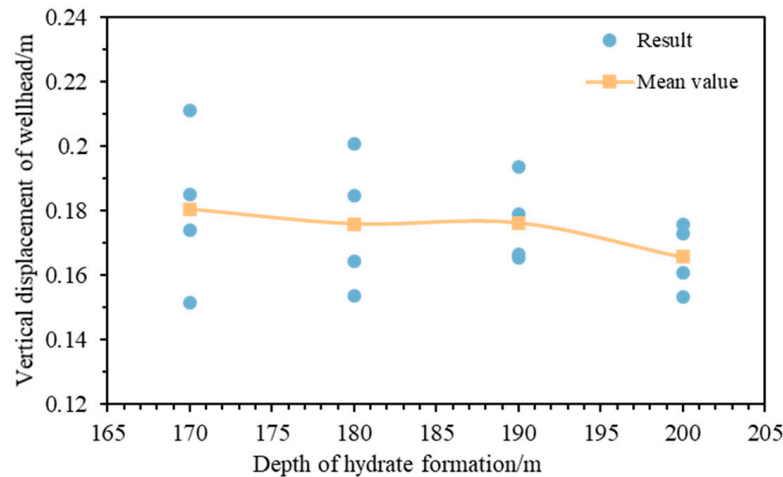


Figure 12. Relationship between subsea wellhead subsidence and depth of hydrate formation.

The reason for this result is that, with the increase of hydrate sediment depth, the overlying formation with larger thickness can bear more load from subsea wellhead casing, while the load borne by hydrate sediment decreases. As a result, the influence of hydrate decomposition on underwater wellhead settlement is reduced.

5. Conclusions

In this paper, a THMC coupling numerical model has been established to analyze the subsidence of wellhead during drilling. In addition, the influence laws of various factors on the stability of subsea wellhead were systematically analyzed. The conclusions drawn from our study are as follows:

(1) Heat transfer between the drilling fluid and hydrate sediment can cause the decomposition of hydrate, which leads to the hydrate sediment compressed and subsea wellhead subsidence. With the increase in the drilling time and drilling fluid temperature, the subsea wellhead subsidence increases gradually.

(2) According to the significance level that affecting the stability of the subsea wellhead, the factors are ranked in a descending order as follows: the thickness of hydrate formation, initial hydrate saturation, overburden depth of hydrate sediment, and mudline temperature, and among them, the mudline temperature insignificantly influences the stability of subsea wellhead.

(3) As the thickness of hydrate formation increases, there is a notable increase in the vertical displacement of the wellhead. Mechanical properties of the dissociated hydrate sediment influence the wellhead stability. The growth of the initial hydrate saturation increases the sediment compression, resulting in larger wellhead subsidence. Moreover, the subsidence of wellhead is negatively correlated with the depth of the hydrate layer.

(4) The actions such as increasing drilling speed or cooling the drilling fluids can reduce the hydrate dissociation and reduce the vertical displacement of wellheads during the drilling of hydrate-bearing formation. It is important to consider hydrate formation thickness, initial hydrate saturation, and hydrate sediment cover depth when planning drilling operations.

Author Contributions: Methodology, Conceptualization, Supervision (Y.C., C.Y. and Z.H.), Software, Investigation, Formal analysis (M.X., J.S., Y.L. and J.Y.), writing—review and editing (M.X.). All authors contributed critically to draft revision. All authors have read and agreed to the published version of the manuscript.

Funding: This research received no external funding.

Data Availability Statement: The datasets used and analyzed during the current study available from the corresponding author on reasonable request.

Acknowledgments: This research is supported by the National Science Foundation Project of China (51974353, 51704311, 51991362) and CNPC's Major Science and Technology Projects (ZD2019-184-003).

Conflicts of Interest: The authors declare no conflict of interest.

References

1. Wood, D.A. Gas hydrate research advances steadily on multiple fronts: A collection of published research (2009–2015). *J. Nat. Gas Sci. Eng.* **2015**, *24*, A1–A8. [[CrossRef](#)]
2. Chand, S.; Minshull, T.A. Seismic constraints on the effects of gas hydrate on sediment physical properties and fluid flow: A review. *Geofluids* **2003**, *3*, 275–289. [[CrossRef](#)]
3. Kvenvolden, K.A. A primer on the geological occurrence of gas hydrate. *Geol. Soc. London Spéc. Publ.* **1998**, *137*, 9–30. [[CrossRef](#)]
4. Yan, C.; Li, Y.; Cheng, Y.; Wei, J.; Tian, W.; Li, S.; Wang, Z. Multifield coupling mechanism in formations around a wellbore during the exploitation of methane hydrate with CO₂ replacement. *Energy* **2022**, *245*, 123283. [[CrossRef](#)]
5. Chong, Z.R.; Yang, S.H.B.; Babu, P.; Linga, P.; Li, X.S. Review of natural gas hydrates as an energy resource: Prospects and challenges. *Appl. Energy* **2016**, *162*, 1633–1652. [[CrossRef](#)]
6. Song, B.; Cheng, Y.; Yan, C.; Lyu, Y.; Wei, J.; Ding, J.; Li, Y. Seafloor subsidence response and submarine slope stability evaluation in response to hydrate dissociation. *J. Nat. Gas Sci. Eng.* **2019**, *65*, 197–211. [[CrossRef](#)]
7. Wang, H.; Wu, P.; Li, Y.; Liu, W.; Pan, X.; Li, Q.; He, Y.; Song, Y. Gas permeability variation during methane hydrate dissociation by depressurization in marine sediments. *Energy* **2023**, *263*, 125749. [[CrossRef](#)]
8. Klauda, J.B.; Sandler, S.I. Global distribution of methane hydrate in ocean sediment. *Energy Fuels* **2005**, *19*, 459–470. [[CrossRef](#)]
9. Sloan, E.D. Gas hydrates: Review of physical/chemical properties. *Energy Fuels* **1998**, *12*, 191–196. [[CrossRef](#)]
10. Moridis, G.J.; Collett, T.S.; Boswell, R.; Kurihara, M.; Reagan, M.T.; Koh, C.; Sloan, E.D. Toward production from gas hydrates: Current status, assessment of resources, and simulation-based evaluation of technology and potential. *SPE Reserv. Eval. Eng.* **2009**, *12*, 745–771. [[CrossRef](#)]
11. Merey, S. Drilling of gas hydrate reservoirs. *J. Nat. Gas Sci. Eng.* **2016**, *35*, 1167–1179. [[CrossRef](#)]
12. McConnell, D.R.; Zhang, Z.; Boswell, R. Review of progress in evaluating gas hydrate drilling hazards. *Mar. Pet. Geol.* **2012**, *34*, 209–223. [[CrossRef](#)]
13. Sun, W.; Pei, J.; Wei, N.; Zhao, J.; Xue, J.; Zhou, S.; Zhang, L.; Kvamme, B.; Li, Q.; Li, H.; et al. Sensitivity analysis of reservoir risk in marine gas hydrate drilling. *Petroleum* **2021**, *7*, 427–438. [[CrossRef](#)]
14. Yan, C.; Ren, X.; Cheng, Y.; Song, B.; Li, Y.; Tian, W. Geomechanical issues in the exploitation of natural gas hydrate. *Gondwana Res.* **2020**, *81*, 403–422. [[CrossRef](#)]
15. Feng, W.; Li, D.; Wang, G.; Song, Y. Wellbore stability of a deep-water shallow hydrate reservoir based on strain softening characteristics. *Geofluids* **2020**, *2020*, 8891436. [[CrossRef](#)]
16. Khormali, A.; Koochi, M.R.; Varfolomeev, M.A.; Ahmadi, S. Experimental study of the low salinity water injection process in the presence of scale inhibitor and various nanoparticles. *J. Pet. Explor. Prod. Technol.* **2022**, *13*, 903–916. [[CrossRef](#)]
17. Yang, S.; Zhang, M.; Liang, J.; Lu, J.; Zhang, Z.; Holland, M.; Schultheiss, P.; Fu, S.; Sha, Z.; the GMGS3 Science Team. Preliminary results of China's third gas hydrate drilling expedition: A critical step from discovery to development in the South China Sea. *J. Fire ICE Methane Hydrate Newsl.* **2015**, *15*, 1–5.
18. Wenlong, L.I.; Deli, G.A.O.; Jin, Y.A.N.G. Challenges and prospect of the drilling and completion technologies used for the natural gas hydrate reservoirs in sea areas. *Chin. J. Oil Drill. Prod. Technol.* **2019**, *41*, 681–689. [[CrossRef](#)]
19. Wan, Y.; Wu, N.; Hu, G.; Xin, X.; Jin, G.; Liu, C.; Chen, Q. Reservoir stability in the process of natural gas hydrate production by depressurization in the shenhu area of the south China sea. *Nat. Gas Ind. B* **2018**, *5*, 631–643. [[CrossRef](#)]
20. Yan, C.; Cheng, Y.; Li, M.; Han, Z.; Zhang, H.; Li, Q.; Teng, F.; Ding, J. Mechanical experiments and constitutive model of natural gas hydrate reservoirs. *Int. J. Hydrogen Energy* **2017**, *42*, 19810–19818. [[CrossRef](#)]
21. Li, Y.; Cheng, Y.; Yan, C.; Song, L.; Liu, H.; Tian, W.; Ren, X. Mechanical study on the wellbore stability of horizontal wells in natural gas hydrate reservoirs. *J. Nat. Gas Sci. Eng.* **2020**, *79*, 103359. [[CrossRef](#)]
22. Zhang, M.; Niu, M.; Shen, S.; Dai, S.; Xu, Y. Review of natural gas hydrate dissociation effects on seabed stability. *Nat. Hazards* **2021**, *107*, 1035–1045. [[CrossRef](#)]
23. Fereidounpour, A.; Vatani, A. An investigation of interaction of drilling fluids with gas hydrates in drilling hydrate bearing sediments. *J. Nat. Gas Sci. Eng.* **2014**, *20*, 422–427. [[CrossRef](#)]
24. Kim, H.C.; Bishnoi, P.R.; Heidemann, R.A.; Rizvi, S.S. Kinetics of methane hydrate decomposition. *Chem. Eng. Sci.* **1987**, *42*, 1645–1653. [[CrossRef](#)]
25. Clarke, M.A.; Bishnoi, P.R. Measuring and modelling the rate of decomposition of gas hydrates formed from mixtures of methane and ethane. *Chem. Eng. Sci.* **2001**, *56*, 4715–4724. [[CrossRef](#)]

26. Yan, C.; Chen, Y.; Tian, W.; Cheng, Y.; Li, Y. Effects of methane-carbon dioxide replacement on the mechanical properties of natural gas hydrate reservoirs. *J. Clean. Prod.* **2022**, *354*, 131703. [[CrossRef](#)]
27. Sun, X.; Mohanty, K.K. Kinetic simulation of methane hydrate formation and dissociation in porous media. *Chem. Eng. Sci.* **2006**, *61*, 3476–3495. [[CrossRef](#)]
28. Liu, X.; Liu, C.; Wu, J. Dynamic characteristics of offshore natural gas hydrate dissociation by depressurization in marine sediments. *Geofluids* **2019**, *2019*, 6074892. [[CrossRef](#)]
29. Sun, J.; Zhang, L.; Ning, F.; Lei, H.; Liu, T.; Hu, G.; Lu, H.; Lu, J.; Liu, C.; Jiang, G.; et al. Production potential and stability of hydrate-bearing sediments at the site GMGS3-W19 in the South China Sea: A preliminary feasibility study. *Mar. Pet. Geol.* **2017**, *86*, 447–473. [[CrossRef](#)]
30. Sun, J.; Ning, F.; Liu, T.; Li, Y.; Lei, H.; Zhang, L.; Cheng, W.; Wang, R.; Cao, X.; Jiang, G. Numerical analysis of horizontal wellbore state during drilling at the first offshore hydrate production test site in Shenhu area of the South China Sea. *Ocean Eng.* **2021**, *238*, 109614. [[CrossRef](#)]
31. Ertekin, T.; Abou-Kassem, J.H.; King, G.R. Basic applied reservoir simulation. *Richardson: Soc. Pet. Eng.* **2001**, *7*, 381.
32. Sun, S.; Yang, Z.; Gu, L.; Lin, H.; Zhang, C. Effect of bubbles on the gas–water migration during gas hydrate dissociation by depressurization. *Fuel* **2023**, *339*, 127429. [[CrossRef](#)]
33. Moridis, G.J. *User's Manual for the Hydrate v1. 5 Option of TOUGH+ v1. 5: A Code for the Simulation of System Behavior in Hydrate-Bearing Geologic Media (No. LBNL-6869E)*; Lawrence Berkeley National Lab.(LBNL): Berkeley, CA, USA, 2014.
34. Yoneda, J.; Masui, A.; Konno, Y.; Jin, Y.; Egawa, K.; Kida, M.; Ito, T.; Nagao, J.; Tenma, N. Mechanical properties of hydrate-bearing turbidite reservoir in the first gas production test site of the Eastern Nankai Trough. *Mar. Pet. Geol.* **2015**, *66*, 471–486. [[CrossRef](#)]
35. Sun, J.; Ning, F.; Lei, H.; Gai, X.; Sánchez, M.; Lu, J.; Li, Y.; Liu, L.; Liu, C.; Wu, N.; et al. Wellbore stability analysis during drilling through marine gas hydrate-bearing sediments in Shenhu area: A case study. *J. Pet. Sci. Eng.* **2018**, *170*, 345–367. [[CrossRef](#)]
36. Miyazaki, K.; Yamaguchi, T.; Sakamoto, Y.; Tenma, N.; Ogata, Y.; Aoki, K. Effect of confining pressure on mechanical properties of sediment containing synthetic methane hydrate. *J. MMIJ* **2010**, *126*, 408–417. [[CrossRef](#)]
37. Sun, X.; Nanchary, N.; Mohanty, K.K. 1-D Modeling of Hydrate Depressurization in Porous Media. *Transp. Porous Media* **2005**, *58*, 315–338. [[CrossRef](#)]
38. Freij-Ayoub, R.; Tan, C.; Clennell, B.; Tohidi, B.; Yang, J. A wellbore stability model for hydrate bearing sediments. *J. Pet. Sci. Eng.* **2006**, *57*, 209–220. [[CrossRef](#)]
39. Selim, M.S.; Sloan, E.D. Heat and mass transfer during the dissociation of hydrates in porous media. *AIChE J.* **1989**, *35*, 1049–1052. [[CrossRef](#)]
40. Chibura, P.E.; Zhang, W.; Luo, A.; Wang, J. A review on gas hydrate production feasibility for permafrost and marine hydrates. *J. Nat. Gas Sci. Eng.* **2022**, *100*, 104441. [[CrossRef](#)]
41. Wei, J.; Cheng, Y.; Yan, C.; Li, Q.; Han, S.; Ansari, U. Decomposition prevention through thermal sensitivity of hydrate formations around wellbore. *Appl. Therm. Eng.* **2019**, *159*, 113921. [[CrossRef](#)]

Disclaimer/Publisher's Note: The statements, opinions and data contained in all publications are solely those of the individual author(s) and contributor(s) and not of MDPI and/or the editor(s). MDPI and/or the editor(s) disclaim responsibility for any injury to people or property resulting from any ideas, methods, instructions or products referred to in the content.